Ultrafast Spectroscopy of the Uranium(IV) and Thorium(IV) Bis(ketimide) Complexes $(C_5Me_5)_2An[-N{=}C(Ph)(CH_2Ph)]_2$ (An = Th, U)

David J. Hilton,*,†,¶ Rohit P. Prasankumar,† Eric J. Schelter,‡ Verner K. Thorsmølle,†,⊥ Stuart A. Trugman,§ Andrew P. Shreve,† Jaqueline L. Kiplinger,‡ David E. Morris,† and Antoinette J. Taylor†

MPA-CINT, MS K771, Los Alamos National Laboratory, Los Alamos, New Mexico, 87545, MPA-10, MS J514, Los Alamos National Laboratory, Los Alamos, New Mexico 87545, T-11, MS B262, Los Alamos National Laboratory, Los Alamos, New Mexico 87545, École Polytechnique Fédérale de Lausanne, CH-1015 Lausanne, Switzerland, and Department of Physics, University of Alabama-Birmingham, Birmingham, Alabama 35211

Received: January 15, 2008; Revised Manuscript Received: June 09, 2008

Ultrafast pump−probe spectroscopic studies have been performed on $(C_5Me_5)_2U[-N{=}C(Ph)(CH_2Ph)]_2$ and $(C_5Me_5)_2Th[-N{=}C(Ph)(CH_2Ph)]_2$ including, for the uranium complex, the first direct measurement of dynamics of electronic deactivation within a 5f-electron manifold. Evidence has been found for strong coupling between the electronic ground state and the f-electron manifold which dominates the dynamics of the excited states of the bis(ketimide) uranium complex. These also demonstrate strong singlet−f manifold coupling, which assists in the deactivation of the photoexcited state of the uranium complex, and provide information on intersystem crossing and internal conversion processes in both complexes.

Introduction

Recently discovered organometallic actinide complexes of general formula $(C_5Me_5)_2An[-N{=}C(R_1)(R_2)]_2$ (An = Th(IV) and U(IV); R_1, R_2 = alkyl or aryl groups) exhibit a rich electronic structure typically seen only in transition-metal chemistry, as a consequence of the strong covalent interactions between the metal valence 5f- and 6d-orbitals and the ketimide ligand-based σ- and π-orbitals.[1–3] This bonding and resultant electronic structure lead to a number of spectral properties that are unique to actinide complexes, including the presence of low-lying metal-to-ligand charge transfer excited states, intensity enhancements in the ligand-field electronic transitions from coupling to the charge transfer excited states, optical emission from predominantly ligand-based singlet and triplet excited states, and resonance-enhanced vibrational Raman scattering from these molecular excited states for complexes of both metals.[3–7] These spectroscopic observations further suggest that energy transfer, relaxation pathway(s) and rates among these various excited electronic states are likely to be equally interesting and their characterization should provide new insight into the role and importance of the intrinsically strong spin−orbit coupling induced by these 5f-elements and the participation or intervention of the ligand-field states derived from the occupied 5f-orbitals in the U(IV) complexes.

We report here results of a comparative ultrafast dynamics investigation of two members of this class of complexes: $(C_5Me_5)_2An[-N{=}C(Ph)(CH_2Ph)]_2$ (An = Th(IV) (**1**) and U(IV) (**2**), Figure 1). Compound **1** shows strong photoluminescence and evidence for the existence of a meta-stable triplet state, while its uranium analogue, **2**, shows no evidence from photoluminescence experiments for any emission at any temperature studied. Ultrafast differential transmission measurements on **1** after photoexcitation with a 150 fs, 3.0 eV pump pulse reveal a multiexponential decay to a long-lived (≫1 ns) excited state, consistent with the photoluminescence experiments. In contrast, ultrafast experiments utilizing a 3.0 eV pump pulse measure a differential transmission in **2** which shows a ∼1 ps relaxation to the ground state. Direct excitation of the 5f-electron ligand-field manifold at 1.0 eV in **2** also shows deactivation to the ground state within ∼1 ps, consistent with experiments utilizing a 3.0 eV pump. Our observations suggest a strong influence of the 5f manifold on the deactivation of the singlet manifold in **2** and provide an explanation for the absence of any long-lived luminescent state in **2**.

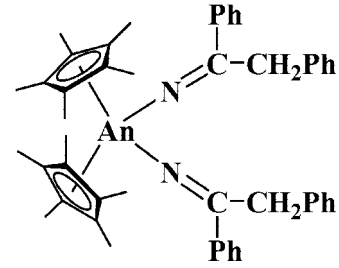

Figure 1. Complexes evaluated in this study: An = Th (**1**), U (**2**); Ph = C_6H_5.

Experimental Methods

Sample Preparation. Reactions and manipulations were performed at 293 K in a recirculating Vacuum Atmospheres model HE-553-2 inert atmosphere (N_2) drybox with a MO-40-2 Dri-Train. Glassware was dried overnight at 423 K before use. Tetrahydrofuran-d_8 was obtained from Cambridge Isotope Laboratories (CIL) and purified by drying with potassium hydride and storage over activated 4 Å molecular sieves prior to use. The complexes $(C_5Me_5)_2Th[-N{=}C(Ph)(CH_2Ph)]_2$ (**1**) and $(C_5Me_5)_2U[-N{=}C(Ph)(CH_2Ph)]_2$ (**2**) (shown in Figure 1)

* Author for correspondence. E-mail: dhilton@uab.edu
† MPA-CINT, MS K771, Los Alamos National Laboratory.
‡ MPA-10, MS J514, Los Alamos National Laboratory.
§ T-11, MS B262, Los Alamos National Laboratory.
⊥ École Polytechnique Fédérale de Lausanne.
¶ Department of Physics, University of Alabama-Birmingham.

10.1021/jp800392b CCC: $40.75
Published on Web 08/06/2008

were prepared according to literature procedures.[1] As depleted uranium (primarily isotope ^{238}U) and natural thorium (isotope ^{232}Th) are weak α-emitters with half-lives of 4.47×10^9 and 1.41×10^{10} years, respectively, for safety, all manipulations and reactions involving these radioactive materials were carried out in monitored fume hoods or in an inert atmosphere drybox in a radiation laboratory equipped with α- and β-counting equipment.

Tetrahydrofuran-d_8 solutions of **1** were calibrated at a photon energy of 3.0 eV (413 nm) to an optical density of 1.0 ± 0.1 for ultraviolet pump experiments. Solutions composed of 65 mg of **1** dissolved in 2.10 g of tetrahydrofuran-d_8 yielded optical densities of 1.0 at 3.0 eV. Tetrahydrofuran-d_8 solutions of **2** were similarly calibrated at an energy of 3.0 eV (413 nm) to an optical density of 1.0 ± 0.1. For experiments utilizing a 3.0 eV pump, 6 mg of **2** was dissolved in 2.60 g of tetrahydrofuran-d_8 yielding a solution with an optical density (O.D.) of 0.9 at 413 nm (3.0 eV). Samples for experiments using mid-infrared excitation were similarly prepared with an O.D. of 1.1 at 1200 nm (∼1.0 eV) from 54 mg of **2** dissolved in 2.63 g tetrahydrofuran-d_8. The absorption of tetrahydrofuran-d_8 in the sample used for mid-infrared excitation was accounted for by referencing the absorption of **1** and **2** to a blank cell of tetrahydrofuran-d_8. Static absorption spectra of the solutions were measured before and after laser irradiation in all cases to check for sample integrity. Post-irradiation measurements indicated partial bleaching and decomposition, presumably due to photoinduced degradation in the experimental conditions. Fresh samples were periodically used after determining the viable lifetimes of given samples under laser irradiation. No change in differential transmission was observed between otherwise identical samples having different irradiation histories, indicating this sample photodegradation does not influence our observations.

Spectroscopic Measurements. Electronic absorption spectral data were obtained for tetrahydrofuran-d_8 solutions of the complexes over the wavelength range 300−1600 nm using a Perkin-Elmer model Lambda 950 UV−visible−near-infrared spectrophotometer. All data were collected in 1 mm path length cuvettes loaded in the Vacuum Atmospheres drybox system described above and run versus a tetrahydrofuran-d_8 reference.

Samples for spectral emission were typically 1−10 mM in toluene or THF and were prepared in the Vacuum Atmospheres drybox system described above; samples consisted of flame-sealed medium-walled NMR tubes (Wilmad 504-PP) in 77 K glass (toluene) or ice (THF) using a liquid-nitrogen optical dewar. A Spex Industries Fluorolog 2 system or a Photon Technology International (PTI) Model QM-4 system was used for the measurements. The former is composed of a 450-W Xe arc lamp CW source, a 0.22-m single-stage excitation monochromator, a 0.22-m double emission monochromator, both with 1200 grove/mm gratings, and a thermoelectrically cooled Hamamatsu R928 photomultiplier detector. The PTI system is composed of 0.2 m single-stage emission and excitation monochromator with 1200 grove/mm gratings. It can be implemented in either a continuous-wave excitation mode using a 75 W Xe arc lamp source, or a pulsed (time-resolved) excitation mode using a Xe flashlamp. Both CW and time-resolved detectors employ Hamamatsu R928 photomultiplier tubes. Spectral resolution in all emission scans was <2 nm and the time resolution was 20 μs.

Ultrafast differential transmission measurements used a Coherent RegA titanium:sapphire regenerative amplifier as a source laser, which produces ∼70 fs pulses at a center photon energy of 1.5 eV and a repetition rate of 250 kHz (4 μs between pulses). The RegA output was sent to a Coherent 9450 optical parametric amplifier (OPA) to generate frequency-doubled ∼150 fs light pulses at 3.0 eV and, by optical parametric generation and amplification, signal and idler pulses tunable from 1.7−2.3 eV. A Coherent 9850 OPA was used in place of the 9450 to generate 1.0 eV pulses for the degenerate pump−probe experiments at this photon energy. The optical excitation average power was 4 mW in the experiment, unless otherwise indicated, and was focused to a ∼180 μm diameter spot onto the cuvette (resulting in an excitation fluence of 63 μJ cm^{-2}). The pump beam in each experiment was modulated at 2.5 kHz using a New Focus model 3501 optical chopper. The transmitted probe beam was passed through an optical filter to block the residual pump beam and measured using an Electro-Optical Systems InGaAs detector (model number: IGA-2.2-010-TE2-H). A Stanford Research Systems SR830 lock-in amplifier was used to measure the photoinduced change in the transmitted probe pulse as a function of time delay measured with respect to the pump pulse, which is accomplished by varying the path length between the pump and probe pulses using an optical delay line. The temporal resolution of the experiment is limited by the cross correlation of the optical pulses to ∼215 fs, while the maximum delay available for these measurements is limited by the length of the optical delay line to be ∼1 ns.

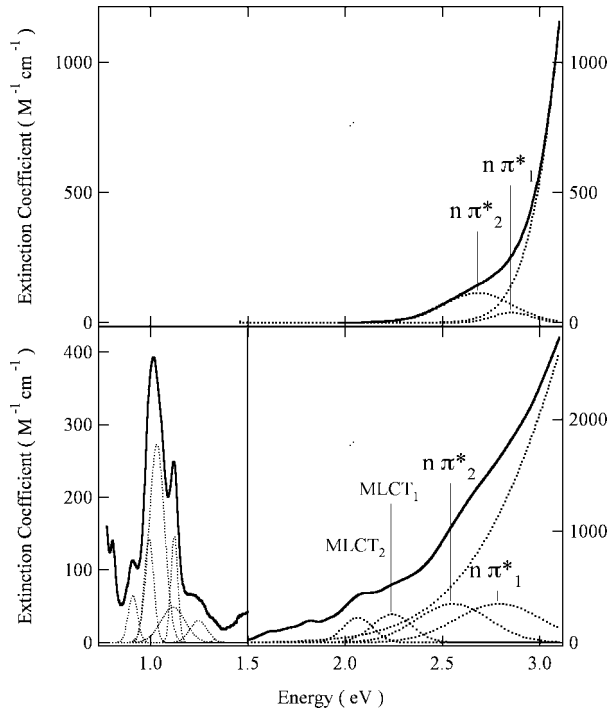

Figure 2. Room-temperature electronic absorption spectra of $(C_5Me_5)_2Th[-N{=}C(Ph)(CH_2Ph)]_2$ (**1**) (top) and $(C_5Me_5)_2U[-N{=}C(Ph)(CH_2Ph)]_2$ (**2**) (bottom) in toluene solution. See text and refs 3 and 7 for discussion and band assignments.

Results

Electronic Absorption and Emission Spectral Results. The absorption spectra at 300 K for **1** and **2**, normalized to sample concentration, are shown in Figure 2. The features apparent in these spectra are consistent across the entire series of bis(ketimide) complexes, $(C_5Me_5)_2An[-N{=}C(R_1)(R_2)]_2$ (An = Th, U; R_1, R_2 = alkyl, aryl), and detailed discussions of the assignments of the electronic transitions in these spectra have been presented previously.[3−7] We briefly summarize these results here as they pertain to complexes **1** and **2**. Note that the component bands

illustrated in these spectral plots (Figure 2) were obtained from unconstrained nonlinear least-squares fits of the raw spectral data using a sum of Gaussian bands in the visible region and a sum of Voigt bands in the NIR region for the spectrum of **2**. Not all component bands required in the fit for **2** are illustrated in Figure 2.

The dominant features in the absorption spectrum of **1** are the two nearly degenerate bands that have been assigned to nonbonding $p_N \rightarrow \pi^*_{C=N}$ transitions (hereafter referred to as nπ*) localized on the ketimide ligands.[7] This assignment is supported by time-dependent density functional theory (TD-DFT) calculations that accurately predict the energy and intensity of these orbitally forbidden, but spin allowed, transitions to the lowest lying singlet states (S_1 at 2.68 eV and S_2 at 2.86 eV).[4,7] The more intense band that tails into the visible portion of the spectrum from ~3 eV is a composite of $\pi\pi$* transitions localized on the C_5Me_5 ligands and the aryl groups on the ketimide ligands. Notably, the nπ* transitions are responsible for the unusual bright yellow color of this thorium complex.[1,4,5] There are no metal-based electronic transitions in the visible or NIR spectral region for **1**, consistent with the absence of metal valence electrons for Th(IV).

The uranium complex **2** also possesses two ketimide ligand-localized transitions of predominantly nπ* character in the same energy region as those for **1**, generating S_1 (2.55 eV) and S_2 (2.79 eV) excited states. These states, too, are consistent with predictions from TD-DFT calculations.[3,4] Our use of singlet (and triplet) labels in complex **2** refers to the ligand-centered transitions, while overall, the $5f^2$ valence electronic configuration of U(IV) also engenders a much richer suite of low-lying excited states, as illustrated in Figure 2. In particular, there are new transitions in the visible spectral region, the most prominent at 2.06 and 2.24 eV, that are assigned to metal-to-$ligand_{ketimide}$ charge transfer transitions (MLCT).[3,4] As noted previously, it is unclear whether each of these transitions leads to a distinct electronic state or whether the individual bands are vibronic components of a transition to the same electronic state.[3] Nonetheless, these are the electronic transitions that give rise to the largest resonance enhancement effect in the vibrational Raman spectrum consistent, with the MLCT assignment.[5] The $5f^2$ valence electronic configuration also gives rise to ligand-field (*f*−*f*) transitions deriving from the $^3H_4$ ground-state manifold in **2**. As shown in Figure 2, the most prominent bands are observed in the NIR spectral region, and most of these bands have anomalously large extinction coefficients for nominally parity forbidden transitions. This intensity enhancement has been attributed to mixing of the MLCT excited state(s) into the ligand-field states by a Herzberg−Teller mechanism.[3] Finally, the high-energy absorption spectrum of **2** is substantially more intense than that of **1**. This increased intensity could derive from additional higher-energy charge-transfer and/or ligand-localized transitions or from the low-energy tail of an unresolved interconfiguration ($5f^2 \rightarrow 5f^16d^1$) transition on the uranium metal center that lies to higher energy.[3] These higher-lying states were not probed in these ultrafast experiments and are not considered in assessing the excited-state relaxation dynamics.

The thorium bis(ketimide) complexes also exhibit luminescence in the visible spectral region when excited in or above the region of the nπ* excited states.[7] Complex **1** is one of the weaker emitters in the series, and no spectral data could be collected in ambient-temperature solutions. However, upon cooling to 77 K, comparable emission spectra are obtained from either tetrahydrofuran ice or toluene glass. Spectral data for **1** at 77 K in a toluene glass are shown in Figure 3. The continuous-wave (CW) excitation spectrum (solid line) obtained while monitoring emission at 2.16 eV (in the T_1 region, vide infra) clearly shows a strong correlation among the singlet states identified in the absorption spectrum and the states responsible for the 77 K emission behavior. The additional structure observed in the excitation spectrum is attributed to resolution of vibronic bands at this lower temperature. The most interesting observation from these emission data comes from a comparison of the CW and time-resolved emission spectra (Figure 3). The CW emission spectrum (dashed line) at 77 K shows clearly a contribution from two distinct states, the higher-energy one being strongly correlated with the S_1 state in the absorption spectrum. However, the time-resolved spectrum obtained with a detection delay of 120 μs reveals that the contribution from this nominal S_1 band has completely disappeared, and only the lower energy band is detected (dotted line). This behavior has been attributed to multiple-state emission from both singlet (S_1) and triplet (T_1) states of the same orbital parentage. The measured lifetime in a toluene glass at 77 K in the energy range of T_1 (2.25 eV) was 410 μs, consistent with a spin-forbidden (triplet) relaxation process.[7] The lifetime of the S_1 state could not be determined with the limited temporal resolution (~20 μs) of the emission system used in these experiments; this limitation will be addressed by results from ultrafast transient absorption measurements presented in the next section.

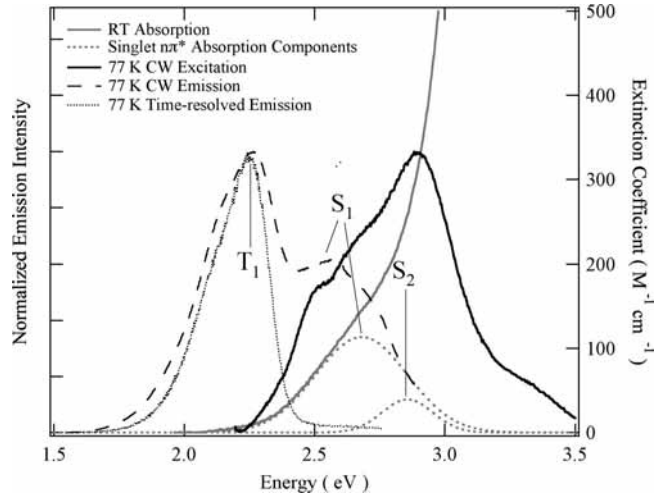

Figure 3. Comparison of 77 K continuous-wave (CW) and time-resolved emission and room-temperature absorption spectral data for $(C_5Me_5)_2Th[-N{=}C(Ph)(CH_2Ph)]_2$ (**1**) in toluene. CW excitation data were obtained while monitoring emission at 2.16 eV. Emission data were obtained while exciting at 2.95 eV. Time-resolved emission data were obtained with a delay of 120 μs and a 1 ms gate width.

Notably, no emission was observed from either tetrahydrofuran or toluene solutions of **2** at any energy between ~1.0 and 2.5 eV and at either ambient-temperature or 77 K, for excitation wavelengths throughout the visible and near UV range. As discussed in further detail below, this observation is consistent with facile relaxation of all excited states of **2** by nonradiative paths back to the ground state.

Ultrafast Experimental Studies of Singlet, Triplet, and 5f Manifold Deactivation. Ultrafast pump−probe spectroscopy is a particularly useful experimental tool for the determination of the dynamics of both radiative and nonradiative deactivation pathways in molecular systems. Techniques such as ultrafast pump−probe transient absorption and time-resolved luminescence can unravel the complex interactions that lead

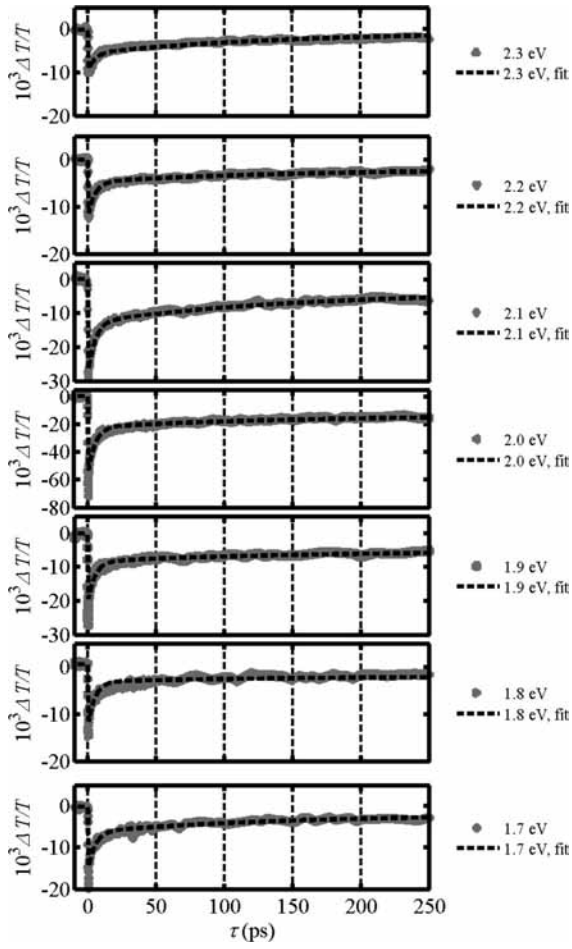

Figure 4. Ultraviolet (3.0 eV) pump−probe as a function of probe energy for $(C_5Me_5)_2Th[-N{=}C(Ph)(CH_2Ph)]_2$ (**1**). The dashed lines represent the best fit of the data to eq 1, as described in the text.

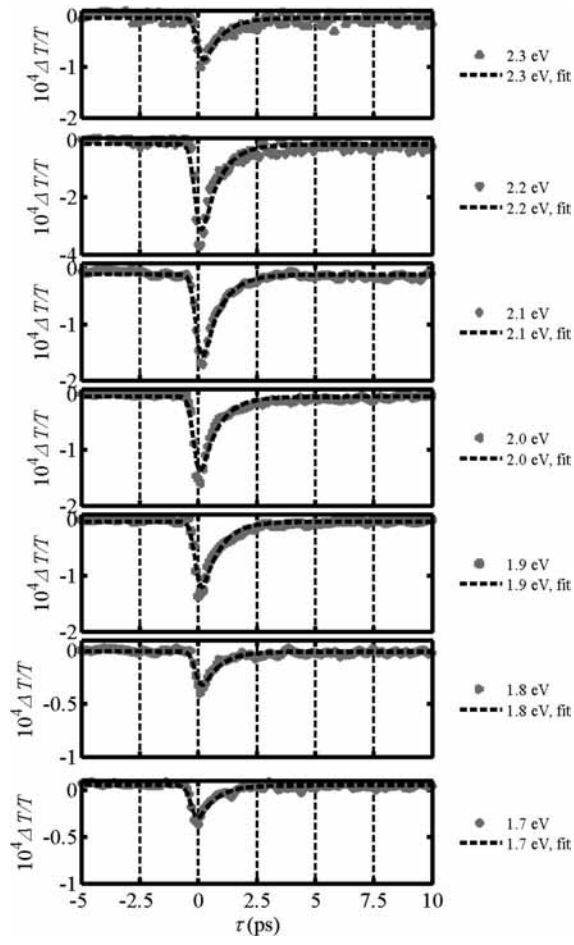

Figure 5. Ultraviolet (3.0 eV) pump−probe as a function of probe wavelength for $(C_5Me_5)_2U[-N{=}C(Ph)(CH_2Ph)]_2$ (**2**). The dashed lines represent the best fit of the data to eq 1, as described in the text.

to observed optical and photophysical properties. However, to date, few direct studies exist of the ultrafast dynamics following photoexcitation of actinide-based complexes.[8,9]

One notable exception is provided by Holten and coworkers who reported subpicosecond relaxation dynamics in the U(IV) porphyrin complexes U(2,3,7,8,12,13,17,18-octaethylporphyrinate)$_2$ (**3**) and U(5,10,15,20-tetraphenylporphyrinate)$_2$ (**4**).[8] These compounds were shown to relax nonradiatively to the ground state within ~1 ps after photoexcitation with a 150 fs pulse centered at 582 nm. These ultrafast dynamics were attributed to a complex deactivation, beginning with an intersystem crossing to the triplet state and followed by relaxation to the ground state by way of the 5f-electron manifold.[8] No comparative data, however, were reported for similar molecules lacking 5f electrons, such as the structurally related Th(IV) compounds,[9] nor were any experiments performed involving direct excitation of states within the 5f-electron manifold.

These previously studied molecular systems possess similar electronic properties to the bis(ketimide) complexes studied in this manuscript. The UV−visible region of the spectra in the uranium porphyrin complexes (**3** and **4**) are dominated by ligand-based electronic transitions.[8] The partially occupied 5f-electron levels in both the uranium porphyrin (**3** and **4**) and ketimide (**2**) systems are energetically situated *between* the highest occupied and lowest unoccupied ligand-based orbitals. This electronic configuration provides a possible deactivation pathway for the ligand-based singlet and triplet manifolds that is unique to these systems and whose influence is currently not well understood. Direct investigation of the dynamics of the 5f-electronic manifold, in addition to dynamic investigations of the singlet and triplet manifolds, could be useful in determining the mechanism responsible for the absence of light emission in **2**. Additionally, a comparative analysis of deactivation pathways in both **1** and **2** could help further elucidate the deactivation mechanisms in both systems, since **1** lacks the low-lying manifold of 5f-electron states.

Compound **1** was excited at 300 K using the frequency doubled (3.0 eV) output of the regenerative amplifier, populating the S_2 state in the singlet manifold. The differential change in transmission ($\Delta T/T$) was then measured as a function of path length delay between the pump pulse and a tunable (1.7−2.3 eV) probe pulse. Figure 4 shows the measured differential transmission at probe energies from 1.7−2.3 eV. These dynamics were fit to a multiexponential decay model, given in eq 1.

$$\frac{\Delta T}{T}(t) = \int_0^\infty \left[A + B_1 \exp\left(\frac{-x}{\tau_1}\right) + B_2 \exp\left(\frac{-x}{\tau_2}\right)\right] \exp\left(\frac{-(t-x)^2}{w^2}\right) \mathrm{d}x \quad (1)$$

Here, the time, t, is measured from the peak of the pump pulse, which occurs at time zero. The amplitudes (lifetimes) of the slow and fast decay components are given by B_1 (τ_1) and B_2 (τ_2), respectively. The effect of the finite excitation (τ_{ex}) and

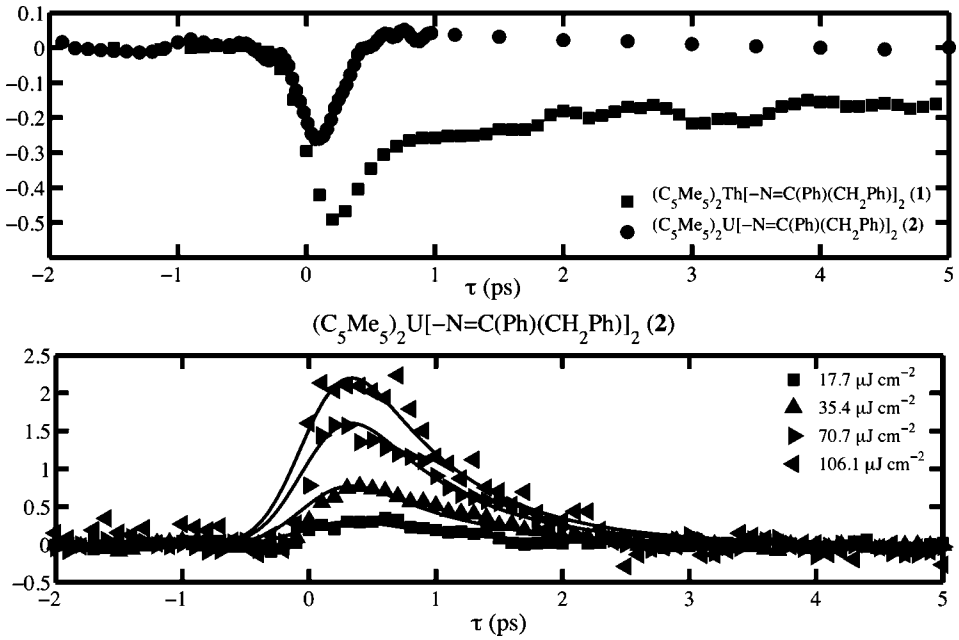

Figure 6. (Top) Optical pump, mid-infrared probe on $(C_5Me_5)_2Th[-N{=}C(Ph)(CH_2Ph)]_2$ (**1**) (square) and $(C_5Me_5)_2U[-N{=}C(Ph)(CH_2Ph)]_2$ (**2**) (circles). (Bottom) Mid-infrared (1.0 eV) pump, mid-infrared (1.0 eV) probe for $(C_5Me_5)_2U[-N{=}C(Ph)(CH_2Ph)]_2$ (**2**) at four excitation fluences; the amplitude scales linearly with excitation fluence. The solid lines represent fits to the model (eq 2) as described in the text.

probe (τ_{pr}) pulse temporal widths is calculated by convolving the model function with a Gaussian function described by a width of w (defined by $w^2 = \tau_{ex}^2 + \tau_{pr}^2$), which accounts for the temporal overlap of the two pulses. Furthermore, as full recovery to the ground state ($\Delta T/T = 0$) is incomplete within the measurement window (~1 ns), a time-independent offset, A, was introduced in eq 1 to account for this. The risetime of our data is limited by the cross correlation width, w, of 215 fs in our experiment; inclusion of a risetime in the numerical fits does not substantially improve the agreement between the data and model. One single set of lifetimes, τ_1 and τ_2, have been extracted from these multiple probe wavelength data using a constrained nonlinear fitting procedure performed on the full set of experimental data.

The solid lines in Figure 4 represent these best-fit curves to this model using these extracted parameters. The initial fast relaxation ($\tau_1 = 5.2 \pm 0.5$ ps) is consistent with the internal conversion within the singlet manifold from the higher order singlet state (S_2) to the lowest level within the excited singlet manifold (S_1). The intermediate lifetime ($\tau_2 = 148 \pm 5$ ps) is consistent with the intersystem crossing from the singlet to the triplet manifold. This assignment is also consistent with the observation of emission from the singlet-to-ground transition at 77 K in **1**, which implies existence of a population in the singlet manifold and not a fast (i.e., on the order of a few picoseconds) intersystem crossing to the triplet. The constant offset is consistent with the long decay times of the metastable triplet states in similar molecular systems and is supported by the measurements of a long-lived photoluminescence at this transition energy in **1**.

The deactivation dynamics of **2** were measured under similar experimental conditions. These results are plotted in Figure 5 and are characterized by an initial decrease in transmission (increase in absorption) whose temporal onset is limited by the pump and probe pulse widths, followed by rapid (~1 ps) decay to equilibrium. These data could be fit to a single exponential decay model, given in eq 2, characterized by a single amplitude, B_1, a relaxation time, τ_1, and accounting for the pump and probe cross correlation by convolving the result with a Gaussian of width, $w = 215$ fs.

$$\frac{\Delta T}{T}(t) = \int_0^\infty B_1 \exp\left(\frac{-x}{\tau_1}\right) \exp\left(\frac{-(t-x)^2}{w^2}\right) dx \qquad (2)$$

The extracted lifetime, τ_1, and amplitude, B_1, at each of the probe energies can be used to produce the numerical fits to eq 2 which are included in Figure 5 as solid lines. The value of $\tau_1 = 0.8 \pm 0.5$ ps is consistent with the various probe wavelength data.

Sample **2** was excited at a pump photon energy of 3.0 eV, which deposits energy into the ligand-centered singlet manifold, and the differential transmission probed at 1.0 eV is plotted in Figure 6 (top, circle). In **2**, the 5f-electron states lead to a ground-state absorption that peaks near 1 eV (Figure 2). Thus, in principle, probing near 1.0 eV could provide direct information on any relaxation pathway that involves coupling through these states. However, the dominant signal in **2** with a 1.0 eV probe following a 3.0 eV pump is an induced absorption, rather than an induced transmission (bleach), and the decay of that absorption is similar to that observed with visible probes. Thus, this experiment likely probes primarily the decay of the singlet or triplet excitations. However, we do note a small induced transmission following decay of the initial induced absorption, and the decay of that transmission occurs on the ~1 ps scale. Given that this decay matches that of an induced transmission observed upon direct excitation of the 5f-electron based absorption features (see below), one plausible assignment is that the initial induced absorption is associated with the initial singlet excitation. This excitation decays to form an excitation within the 5f-electron states, corresponding to a small induced transmission at the 1.0 eV probe wavelength. This 5f excitation then, subsequently, also rapidly decays to the ground state. In contrast, photoexcitation of **1** under the same experimental conditions, also plotted in Figure 6 (top, squares), shows qualitatively similar dynamics to the visible probe data presented in Figure 4, where an initial fast decay was

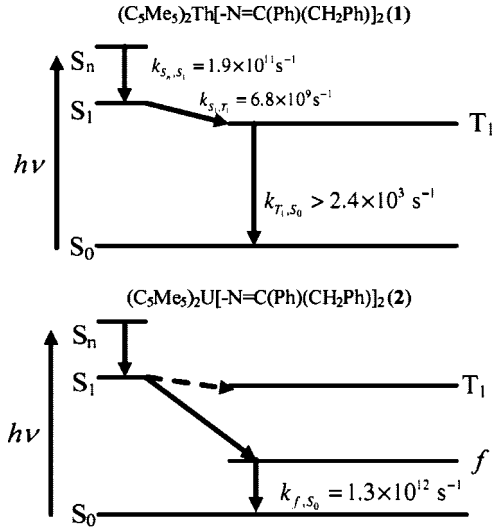

Figure 7. Energy level diagrams for $(C_5Me_5)_2Th[-N{=}C(Ph)(CH_2Ph)]_2$ (**1**) and $(C_5Me_5)_2U[-N{=}C(Ph)(CH_2Ph)]_2$ (**2**). For **1**, the rate constants extracted from the data are presented. For **2**, the decay from the ligand-centered singlet state is found to proceed directly through the 5f-electron manifold of states based on the observed data and the comparative analysis to the dynamics observed in **1**; rate constants as determined by our data are provided. The absence of photoluminescence in **2** is a consequence of this alternate decay pathway, which prevents a long-lived population of the ensemble of molecules in the ligand-centered excited T_1 state. The rate constants determined from the experimental data in ambient conditions are included on the diagram.

followed by an intermediate lifetime and, subsequently, a transition to a long-lived state that decays to the ground state with a lifetime longer than the scanning range of our experiment (≫1 ns). No induced transmission (i.e., reduction in absorption) is observed at any time, corresponding to the absence of ground-state absorption at 1.0 eV for complex **1**.

In order to verify the influence of a 5f-electron deactivation pathway on the electronic structure of **2**, we employ degenerate ultrafast pump−probe spectroscopy to study the differential transmission of an ultrashort probe pulse after photoexcitation with a 1.0 eV pump pulse, which *directly* excites carriers into the 5f-electron manifold, isolating this manifold from processes involving the excited singlet manifold states. As a result, the dynamics of the coupling between the singlet and 5f-electron manifolds previously discussed above are eliminated, and the observed experimental results depend solely on the coupling between the 5f manifold and the ground state.

The molar concentration of **2** for this experiment was different than for the previous measurement and was chosen to produce a sample with an optical density of ∼1 at the pump photon energy (1.0 eV). Compound **2** was excited with a mid-infrared pump pulse (1.0 eV, 200 fs) using the output of an OPA operating in the near-infrared. A portion of this beam was split from the main pump beam, cross-polarized, and used to probe the differential transmission ($\Delta T/T$) induced by the optical pump pulse as a function of delay between the pump and probe pulses. In Figure 6 (bottom), the measured change in transmission as a function of delay at a pump excitation fluence of 18, 35, 71, and 106 μJ cm^{-2} are plotted, which shows an initial increase in transmission (reduction in absorption) with a risetime limited by the cross correlation of the pump and probe pulses (215 fs).

These were fit with eq 2 in order to extract the amplitudes and lifetimes from the experimental data. The amplitude of the differential transmission is a linear function of input optical fluence, indicating that the experiment has been performed below the saturation limit. The near-infrared dynamics reported here result from **2** and not from absorption in the tetrahydrofuran-d_8 solvent, which shows no significant measured differential transmission under the same experimental conditions. Similar experiments performed under the same conditions using **1** show results consistent with those in tetrahydrofuran-d_8 alone, which we attribute to the absence of absorption at these pump energies of the unexcited molecule, as shown in Figure 2.

Discussion

The observed temporal dynamics were fit using simplified four- and five-level systems for complexes **1** and **2**, respectively, shown in Figure 7. For complex **1**, the four-level system consists of the ground state (S_0), first singlet level (S_1), a higher singlet level (S_n), and the first triplet state (T_1). Optical excitation at 3.0 eV from the ground state results in an initial excitation to a higher singlet level (S_n), followed by relaxation to the ground state via the first singlet state and the first triplet state.

$$\begin{aligned}
\frac{dN_{S_n}}{dt} &= +\sigma I(t)N_{S_0} - k_{S_n,S_1}N_{S_n}\\
\frac{dN_{S_1}}{dt} &= +k_{S_n,S_1}N_{S_n} - k_{S_1,T_1}N_{S_1}\\
\frac{dN_{T_1}}{dt} &= +k_{S_1,T_1}N_{S_1} - k_{T_1,S_0}N_{T_1}\\
\frac{dN_{S_0}}{dt} &= +k_{T_1,S_0}N_{T_1} - \sigma I(t)N_{S_0}
\end{aligned} \tag{3}$$

Here, $I(t)$ is the temporal profile of the optical pump pulse and σ is the absorption cross section at the pump wavelength (eqs 3). The internal conversion rate ($S_n \rightarrow S_1$) is given by k_{S_n,S_1}, the intersystem crossing ($S_1 \rightarrow T_1$) rate is k_{S_1,T_1}, and the first triplet state rate constant ($T_1 \rightarrow S_0$) is given by k_{T_1,S_0}. Deactivation pathways between alternate states not written here, most notably a direct intersystem crossing from S_n to the triplet manifold or a direct internal conversion of S_1 to S_0, are not explicitly considered. As an additional simplification, we also neglect the energy splitting of the vibrational levels within these electronic states.

The following general picture is consistent with the observed dynamics in complex **1**. The dynamics are characterized by an initial decay (5.2 ps), considered to be dominated by the S_n to S_1 internal conversion, followed by a second relaxation of $\tau_1 =$ 148 ps, considered to reflect the S_1 to T_1 intersystem crossing (but possibly including contributions from the S_1 to S_0 internal conversion process not considered here if the yield of triplet state formation is less than unity). The longest relaxation, which occurs on a time scale ≫1 ns, too long to be directly observed with our apparatus, must reflect triplet-to-ground-state relaxation. At room temperature, this process occurs within the separation between pulses in our system (4 μs for a 250 kHz repetition rate laser). The lifetime of this metastable state has been measured in a separate time-resolved photoluminescence experiment as 410 μs at 77 K, as discussed above. Although the corresponding ambient-temperature photoluminescence measurements could not be performed, such a lifetime would be expected to be shorter. Further experiments studying the photoluminescence using either more sensitive, photon-counting

techniques or an ultrafast pump probe experiment capable of longer delay scans would be needed to determine this lifetime at 300 K.

For complex **2**, the four-level system used for complex **1** is extended to include the 5f level, shown to exist 1.0 eV above the ground state (see Figure 2). Initial excitation into the singlet manifold proceeds via a state similar to that of complex **1**, but, with the addition of the MLCT states (shown in Figure 2), the singlet manifold is likely to be more complex in **2**. In any case, TD-DFT[3,4] calculations support the assignment of singlet−triplet energy level structure ($n\pi^*$) in **1** and its extension to **2** with additions for MLCT and the 5f-electron manifold. Equations 4 summarize the deactivation pathways proposed for **2** after photoexcitation at 3.0 eV, which extend the four-level system used for **1** to include the influence of the 5f manifold.

$$\begin{aligned}
\frac{dN_{S_n}}{dt} &= +\sigma I(t)N_{S_0} - k_{S_n,S_1}N_{S_n} \\
\frac{dN_{S_1}}{dt} &= +k_{S_n,S_1}N_{S_n} - k_{S_1,T_1}N_{S_1} - k_{S_1,f}N_{S_1} \\
\frac{dN_{T_1}}{dt} &= +k_{S_1,T_1}N_{S_1} - k_{T_1,S_0}N_{T_1} - k_{T_1,f}N_{T_1} \\
\frac{dN_f}{dt} &= +k_{S_1,f}N_{S_1} + k_{T_1,f}N_{T_1} - k_{f,S_0}N_f \\
\frac{dN_{S_0}}{dt} &= +k_{T_1,S_0}N_{T_1} + k_{f,S_0}N_f - \sigma I(t)N_{S_0} \qquad (4)
\end{aligned}$$

The additional rate constant, $k_{S_1,f}$, introduced here represents the direct coupling rate between the first singlet level and the 5f manifold, while, $k_{T_1,f}$ represents the relaxation rate between the triplet and 5f manifolds. The relaxation rate between the 5f manifold and the ground state is given here by the rate constant, k_{f,S_0}.

Equations 4 do not permit the direct determination of the deactivation pathway based on the 3.0 eV pumped data measured in compound **2** alone. The ambiguity here is the pathway by which the photoexcitation, which is initially into the excited singlet manifold, returns to the ground state within ~1 ps. This determination is complicated by the fact that several different deactivation pathways through the 5f manifold are possible in **2,** in addition to the intersystem crossing observed in **1.** Any relaxation rate measured via excitation at 3.0 eV will potentially depend on the rates of internal conversion, intersystem crossing, as well as the dynamics of the coupling between the singlet and triplet manifolds to the 5f level.

Direct excitation of the 5f-electron manifold permits the independent determination of the coupling between 5f and the ground state that cannot unambiguously be determined from the optical and ultraviolet frequency pump−probe experiments. Direct excitation into the 5f manifold can be described by significantly simplified rate equations, as compared to eqs 4.

$$\begin{aligned}
\frac{dN_f}{dt} &= +\sigma I(t)N_{S_0} - k_{f,S_0}N_f \\
\frac{dN_{S_0}}{dt} &= +k_{f,S_0}N_f - \sigma I(t)N_{S_0} \qquad (5)
\end{aligned}$$

Thus, we see that this experiment (Figure 6) isolates the deactivation rate (k_{f,S_0}) from the 5f manifold to the ground state. The measured experimental data shown in Figure 6 can then be fitted with eqs 5 to determine a lifetime of 0.8 ± 0.5 ps.

It is clear from these data that deactivation in **2** after photoexcitation at 3.0 eV proceeds by the following general mechanism: an internal conversion within the excited singlet manifold, a subsequent direct deactivation to the 5f manifold, followed by a rapid deactivation to the ground state. This mechanism is summarized in Figure 7, which shows this simplified model of the singlet, triplet and 5f manifold energy structure of **1** and **2**, as well as the relevant deactivation pathways, as determined in our experiments. Based on the comparative analysis of the experimental data in **2** with those taken in similar experiments in **1**, as well as the direct excitation of the 5f manifold in **2**, we can rule out any significant deactivation to the triplet manifold, as the observed intersystem crossing rate in **1** is too small (i.e., the lifetime is too long) to account for the ~1 ps deactivation observed in **2** (assuming comparable rates of intersystem crossing in these closely related complexes). While this lifetime is significantly shorter than the internal conversion rate in **1** (0.8 ps versus 5.2 ps), the additional MCLT states (see Figure 2, bottom) present in **2** may provide additional pathways for internal conversion, resulting in faster internal conversion in **2** than in **1**. The lack of measurable photoluminescence in **2** is also consistent with the lack of a significant population buildup in the triplet manifold, due to the presence of an alternate, nonradiative deactivation pathway by way of the 5f manifold, as well as the rapid deactivation of the energy deposited in the singlet manifold by this same mechanism.

In summary, the first ultrafast studies of the 5f-electron manifold in $(C_5Me_5)_2U[-N{=}C(Ph)(CH_2Ph)]_2$ and $(C_5Me_5)_2Th[-N{=}C(Ph)(CH_2Ph)]_2$ have been performed using ultrafast pump−probe spectroscopy. We find evidence for strong coupling between the electronic ground state and the 5f-electron manifold in these molecular actinide complexes and show that this coupling dominates the dynamics of the excited states of these molecules. These results are the first direct studies of the deactivation dynamics in the 5f-electron manifold and its influence on the rapid deactivation of the singlet manifolds in actinide systems.

Acknowledgment. For financial support of this work, we acknowledge LANL (Director's and Frederick Reines PD Fellowships to E.J.S.), the LANL G.T. Seaborg Institute (PD Fellowship to E.J.S.), the LANL Laboratory Directed Research and Development program, and the Division of Chemical Sciences, Office of Basic Energy Sciences, Heavy Element Chemistry program. This work was performed, in part, at the Center for Integrated Nanotechnologies, a U.S. Department of Energy, Office of Basic Energy Sciences user facility. Los Alamos National Laboratory, an affirmative action equal opportunity employer, is operated by Los Alamos National Security, LLC, for the National Nuclear Security Administration of the U.S. Department of Energy under contract DE-AC52-06NA25396.

References and Notes

(1) Jantunen, K. C.; Burns, C. J.; Castro-Rodriguez, I.; Da Re, R. E.; Golden, J. T.; Morris, D. E.; Scott, B. L.; Taw, F. L.; Kiplinger, J. L. *Organometallics* **2004**, *23*, 4682–4692.

(2) Kiplinger, J. L.; Morris, D. E.; Scott, B. L.; Burns, C. J. *Organometallics* **2002**, *21*, 3073–3075.

(3) Schelter, E. J.; Yang, P.; Scott, B. L.; Thompson, J. D.; Martin, R. L.; Hay, P. J.; Morris, D. E.; Kiplinger, J. L. *Inorg. Chem.* **2007**, *46*, 7477–7488.

(4) Clark, A. E.; Martin, R. L.; Hay, P. J.; Green, J. C.; Jantunen, K. C.; Kiplinger, J. L. *J. Phys. Chem. A* **2005**, *109*, 5481–5491.

(5) Da Re, R. E.; Jantunen, K. C.; Golden, J. T.; Kiplinger, J. L.; Morris, D. E. *J. Am. Chem. Soc.* **2005**, *127*, 682–689.

(6) Morris, D. E.; Da Re, R. E.; Jantunen, K. C.; Castro-Rodriguez, I.; Kiplinger, J. L. *Organometallics* **2004**, *23*, 5142–5153.

(7) Schelter, E. J.; Yang, P.; Scott, B. L.; Da Re, R. E.; Jantunen, K. C.; Martin, R. L.; Hay, P. J.; Morris, D. E.; Kiplinger, J. L. *J. Am. Chem. Soc.* **2007**, *129*, 5139–5152.

(8) Bilsel, O.; Milam, S. N.; Girolami, G. S.; Suslick, K. S.; Holten, D. *J. Phys. Chem.* **1993**, *97*, 7216–7221.

(9) Bilsel, O.; Rodriguez, J.; Milam, S. N.; Gorlin, P. A.; Girolami, G. S.; Suslick, K. S.; Holten, D. *J. Am. Chem. Soc.* **1992**, *114*, 6528–6538.

JP800392B